

# Analytical solutions for single and multiple scattering from rib-stiffened plates in water

Hesam Bakhtiary Yekta and Andrew N. Norris<sup>1</sup>

<sup>1</sup>*Department of Mechanical & Aerospace Engineering,  
Rutgers University, Piscataway, NJ 08854, USA*

(Dated: March 22, 2024)

The interaction of an acoustic plane wave with a pair of plates connected by periodically spaced stiffeners in water is considered. The rib-stiffened structure is called a “flex-layer” because its low frequency response is dominated by bending stiffness. The quasi-static behavior is equivalent a homogeneous layer of compressible fluid, which we identify as air for the purposes of comparison. In this way an air layer is acoustically the same as a pair of thin elastic plates connected by a periodic spacing of ribs. At discrete higher frequencies the flex-layer exhibits perfect acoustic transmission, the cause of which is identified as fluid-loaded plate waves propagating back and forth between the ribs. Both the low and finite frequency behavior of the flex-layer are fully explained by closed-form solutions for reflection and transmission. The analytical model is extended to two flex-layers in series, introducing new low and high frequency phenomena that are explained in terms of simple lumped parameter models.

## I. INTRODUCTION

Interaction of sound with rib-reinforced plates is a long-standing topic of interest related to acoustical properties of walls, floors, partitions, sound absorbing panels and other structural elements. Many different model configurations have been considered, including: infinite plates with a single rib [1–4], multiple ribs [5], periodic ribs [6–9] or resonators [10]; finite ribbed plates [11–14], and fully three-dimensional models of a rib-stiffened plates [15–17]. The objective here is an analytical solution for the transmission and reflection of underwater sound from two infinite thin plates in parallel with periodic rib stiffening. Our interest in this structure was motivated by the observation that it behaves at low frequency as an equivalent spring-like layer. This behavior contrasts with the low frequency mass law observed for panels in air [18, 19]. For this reason we call the structure a “flex-layer” because of its low frequency stiffness-dominated behavior.

Our focus is the acoustic properties of a pair of infinitely long fluid-loaded plates connected by periodically spaced rib-stiffeners situated in an infinite acoustic fluid (water). We develop closed-form solutions of the reflection and transmission for the pair of plates and also for a system comprising two pairs of plates separated by a water gap. The solution for the latter  $n = 2$  system is found by considering the single scattering problem for an infinite set of evanescent plane waves that are related to the incident plane wave by the Bragg condition. We obtain infinite sized reflection and transmission matrices that can be combined to obtain the response from any number  $n \geq 2$  of plate pairs. The fundamental solution method takes advantage of the infinite periodicity, enabling closed-form solution through the use of the Poisson Summation formula, which has been used to advantage previously in similar problems for vibration [20], sound radiation [21–23] and reflection and transmission

[6, 18, 24].

The paper proceeds as follows. The flex-layer model is introduced in Section II and is shown to be acoustically equivalent at low frequency to a layer of air in water. A full frequency analytical solution for the acoustical response of the flex-layer is developed in Section III. The solution as a sum of symmetric and antisymmetric partial solutions is, to our knowledge, novel, and leads to expressions for equivalent plate impedances. The analytical model is compared with full scale simulation and its transmission properties are discussed in Section IV. Transmission through a pair of flex-layers separated by water is considered in Section V using a new type of analytical solution. Conclusions and future directions are presented in Section VI.

## II. THEORY: LOW FREQUENCY FLEX-LAYER

The rib-stiffened structure, of which a section is shown in Fig. 1(a), comprises parallel plates a distance  $l_r$  apart, and periodically spaced ribs separated by  $2b$ . We are interested in how a plane wave incident from the semi-infinite water region on the right is reflected and transmitted. Before presenting the full solution in Section III we first give a simple solution for the scattering problem in the low frequency or “quasi-static” frequency range.

In the quasi-static regime the frequency is low enough that the dominant deformation mechanism of the plates is bending due to an imposed effectively static pressure, with the entrained air having negligible influence. Hence the name “flex-layer” for the rib-stiffened structure. The deformation between two ribs can be modeled as a clamped-clamped plate, as in Fig. 2. The plate of thickness  $h$  is under pressure  $p_0$  on one side and subject to rigid line constraints in the  $x$ -direction spaced a distance  $2b$  apart (for the purposes of the quasi-static model the effect of a rib stiffener is assumed to be approximated by

a rigid constraint). The plate displacement  $w(y)$  satisfies the Euler-Bernoulli plate equation (the static version of Kirchhoff plate theory)

$$Dw''''(y) = p_0, \quad -b \leq y \leq b \quad (1)$$

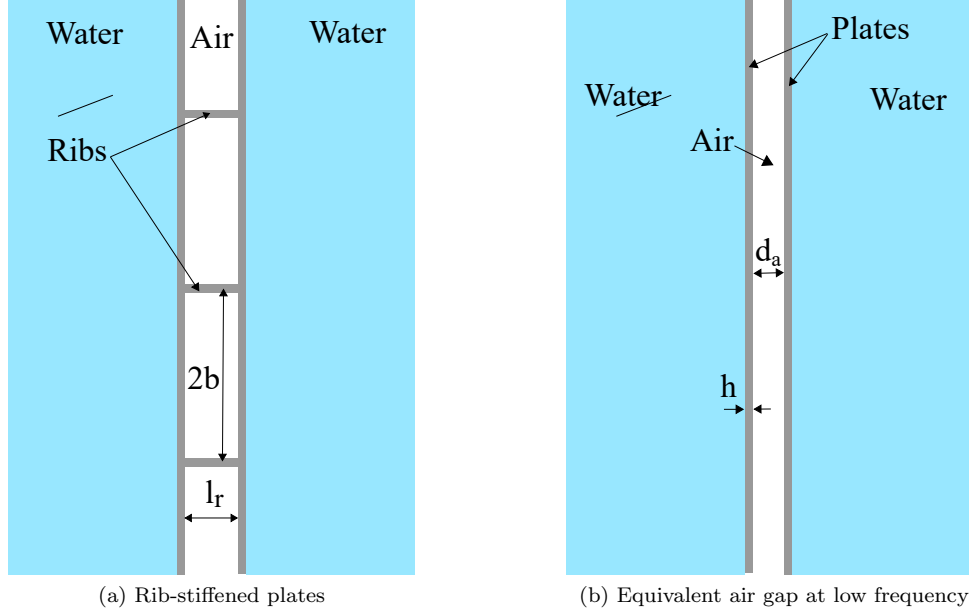


FIG. 1. (a) Flex-layer model of two plates with connecting ribs. (b) Equivalent quasi-static air gap, including two thin elastic plates acting to maintain the air-water separation.

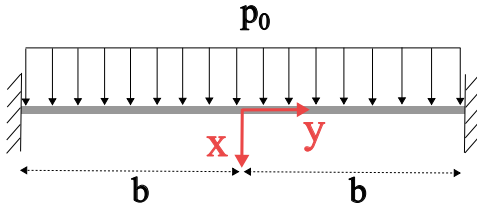


FIG. 2. Clamped-clamped plate under a quasi-static pressure  $p_0$ .

Solving Eq. (1) with the boundary conditions  $w(\pm b) = 0$ ,  $w'(\pm b) = 0$ , yields  $w(y) = p_0(y^2 - b^2)^2/(24D)$ . Since there are two such plates with rigid constraints connecting them, and subject to pressure  $p_0$  on both sides, the change in internal volume over an area  $A$  of the plates comprising a length in the  $z$ -direction and the span  $-b \leq y \leq b$  is  $2Aw_{av}$ , where  $w_{av}$  is the average displacement. The average change in distance separating the plates is therefore  $\Delta L = 2w_{av}$ , or

$$\Delta L = \frac{2}{45} \frac{b^4}{D} p_0. \quad (2)$$

A slightly larger value is found for  $\Delta L$  if the Timoshenko (or equivalently, Mindlin) plate theory is used instead

where  $D = E_p I / (1 - \nu^2)$ ,  $I = h^3 / 12$ ,  $E_p$  is the plate Young's modulus and  $\nu$  the Poisson's ratio.

of the Euler-Bernoulli theory. The relative difference is, however, negligible; see Appendix A.

The same  $\Delta L$  could be obtained with a uniform "spring-layer". In order to make this realistic, consider a thin layer of air separating two half-spaces of water, as shown in Fig. 1(b). The air gap acts at low frequencies as an effective linear spring, with stiffness proportional to the air bulk modulus,  $K_a$ , and inversely proportional to the gap width,  $d_a$ . The additional rigid plates in Fig. 1(b) are introduced as separators between the air and water and do not change the main effect of the air gap as an effective spring. Low frequency here means that the acoustic wavelength in the air gap is much greater than the gap width  $d_a$ . This translates to frequencies  $f \ll c_a/d_a$  where  $c_a = \sqrt{K_a/\rho_a}$  is the speed of sound in air and  $\rho_a$  is the density. In order to quantify the low frequency, or equivalently quasi-static, response consider the two plates subject to static pressure  $p_0$  (positive or negative). The resulting change in thickness of the air gap is

$$\Delta L_a = \frac{d_a}{K_a} p_0. \quad (3)$$

The flex-layer and air gap have equal compliance (or

it's inverse, stiffness) if Eqs. (2) and (3) agree, i.e. if

$$\frac{K_a}{d_a} = \frac{15 h^3}{8 b^4} \frac{E_p}{(1-\nu^2)}. \quad (4)$$

This can be considered a constraint on the three lengths  $b$ ,  $h$  and  $d_a$  for a given plate material. We assume the plates are Aluminum ( $E_p = 70$  GPa,  $\nu = 0.334$ ), and using  $K_a = 0.134$  MPa implies the relation  $b = 32.40 (h^3 d_a)^{1/4}$ . Assuming plates of thickness  $h = 1$  mm, then for different value of  $d_a$  (0.5mm, 1 mm, 2 mm),  $b$  is 2.72 cm, 3.24 cm, and 3.85 cm, respectively.

The equivalence of the flex-layer and the air gap is demonstrated in Fig. 3 which shows the fractional energy transmission of both systems at low frequencies for normal incidence. Also shown is the transmitted energy across a spring layer of stiffness  $\kappa$ , for which the reflection and transmission coefficients are:

$$R = \frac{\frac{i\omega}{\kappa}}{\frac{2}{Z} - \frac{i\omega}{\kappa}}, \quad T = \frac{\frac{2}{Z}}{\frac{2}{Z} - \frac{i\omega}{\kappa}} \quad (5)$$

where  $Z = \rho c$  and  $\kappa = K_a/d_a$  for the air gap. Alternatively,  $\kappa$  can be related to the flex-layer parameters via Eq. (4). This indicates that the quasi-static hypothesis and analogy with the air gap is valid at low frequencies, and that the reflection and transmission depends only on the effective stiffness  $\kappa$ .

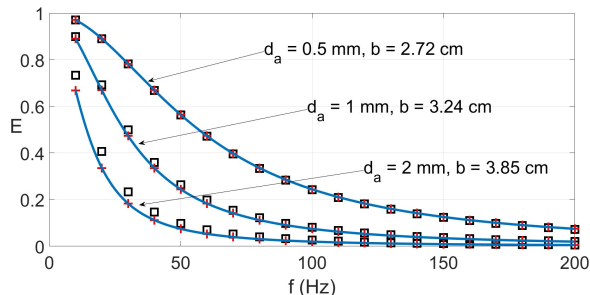


FIG. 3. Transmitted energy ratio  $E = |T|^2$  vs frequency for normal incidence. Solid lines are obtained using Eq. (5), while  $\square$  and  $+$  are obtained using FEM (COMSOL) for the air gap model and flex-layer model, respectively. The plates are Aluminum with  $h = 1$  mm, and the rib half-spacing  $b$  is found using Eq. (4). The non-dimensional acoustic wavenumber  $kb$  where  $k = \omega/c$  is less than 0.033 for the cases shown, implying that the pressure variation along the surface is minimal for non-normal incidence. The curves are therefore independent of the angle of incidence.

We next describe an analytical model for acoustic scattering from the flex-layer that is valid beyond the quasi-static regime.

### III. FULL DYNAMIC MODEL OF SCATTERING FROM A FLEX-LAYER

The periodicity of the flex-layer system of Fig. 4 in the  $y$ -direction introduces the possible generation of re-

flected and transmitted waves with all  $y$ -wavenumbers commensurate in the unit wavenumber  $2\pi/d$  where  $d = 2b$ . We consider oblique plane wave incidence at angle  $\theta_0$  from the normal, with  $y$ -wavenumber  $k \sin \theta_0$  where  $k = \omega/c$ . This can then give rise to waves with wavenumbers in the  $y$  and  $x$  directions, respectively,

$$k_m = k \sin \theta_0 + 2\pi \frac{m}{d}, \quad (k_x)_m = (k^2 - k_m^2)^{1/2}, \quad (6)$$

for all  $m \in \mathbb{Z}$  with the square root either positive real or positive imaginary. If the flex-layer interacts with another scatterer, e.g. another flex-layer or a material interface, the resulting multiple scattering will involve incidence on the flex-layer by all  $y$ -wavenumbers. With that purpose in mind - see Section V - we formulate the problem in a general sense of a single flex-layer incident by  $y$ -wavenumber  $k_n$  for some specific  $n$ .

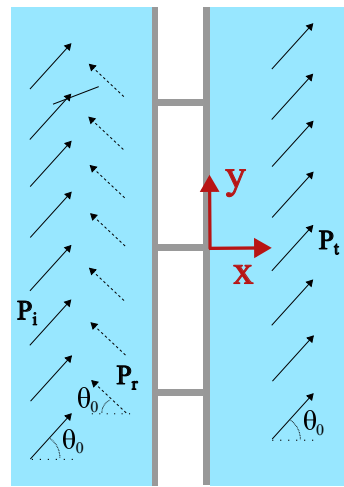


FIG. 4. Incident, reflected, and transmitted waves in Water-Flex-Water model

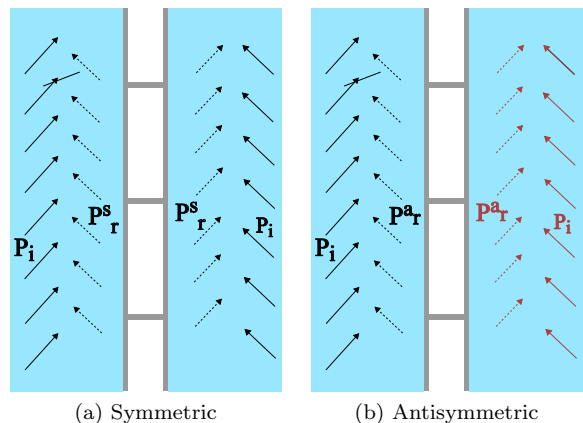


FIG. 5. The separate symmetric and antisymmetric scattering problems. Red indicates negative.

The problem as depicted in Fig. 4 contains incident, reflected, and transmitted waves. The solution is ob-

tained by splitting the scattering problem into distinct cases: symmetric and antisymmetric, see Fig. 5.

### A. Symmetric scattering from a single flex-layer

The total acoustic pressure is assumed to comprise an incident wave of  $y$ -wavenumber  $k_n$ :

$$p(x, y) = p_0 \left[ e^{i(-(k_x)_n|x|+k_n y)} + \sum_{m=-\infty}^{\infty} R_{mn}^{(s)} e^{i((k_x)_m|x|+k_m y)} \right] \quad (7)$$

where  $R_{mn}^{(s)}$  are the symmetric scattering matrix elements. We only need to consider scattering in either  $x > 0$  or  $x < 0$  from a single periodically constrained plate. We look at the  $x > 0$  problem. The setup is a plate on the  $y$ -axis, fluid in  $x > 0$ , and  $(2b =) d$ -periodic normal force constraints on the plate at  $y_m = md$ ,  $m = 0, \pm 1, \pm 2, \dots$ . The following is motivated by Stepanishen's fundamental solution for plane wave incidence on an infinite plate with periodic stiffeners [6].

The total acoustic pressure of Eq. (7) is expressed as

$$p(x, y) = p_0 e^{i(-(k_x)_n x + k_n y)} + p_0 e^{i((k_x)_n x + k_n y)} + p_s(x, y) \quad (8)$$

so that the incident and rigidly reflected terms give zero normal velocity on the plate. The plate normal velocity,  $v(y) = v_x(0, y)$  is related to the additional pressure  $p_s$  by the momentum equilibrium equation in the  $x$ -direction:  $i\omega\rho v(y) = \frac{\partial p_s}{\partial x}(0, y)$ . Introducing the  $y$ -transform,

$$\begin{aligned} \hat{V}(k_y) &= \int_{-\infty}^{\infty} v(y) e^{-i k_y y} dy, \\ v(y) &= \frac{1}{2\pi} \int_{-\infty}^{\infty} \hat{V}(k_y) e^{i k_y y} dk_y, \end{aligned} \quad (9)$$

it follows that the additional scattered pressure is related to the normal velocity by

$$p_s(x, y) = \frac{1}{2\pi} \int_{-\infty}^{\infty} \hat{Z}_f(k_y) \hat{V}(k_y) e^{i(\sqrt{k^2 - k_y^2} x + k_y y)} dk_y \quad (10)$$

where  $\hat{Z}_f$  is a fluid impedance

$$\hat{Z}_f(k_y) = \rho\omega / (k^2 - k_y^2)^{1/2}. \quad (11)$$

The plate displacement in the  $x$ -direction,  $w(y) = (-i\omega)^{-1}v(y)$ , satisfies

$$\begin{aligned} Dw''''(y) - \rho_s h \omega^2 w(y) &= -2p_0 e^{i k_n y} - p_s(0, y) \\ &\quad - Z_0 v(y) \sum_{m=-\infty}^{\infty} \delta(y - y_m). \end{aligned} \quad (12)$$

This assumes Kirchhoff plate theory; the analysis for the alternative Mindlin plate model is given in Appendix B.

The first two forcing terms in Eq. (12) are from the fluid pressure and the final term in (12) represents the forcing from the rib constraints, with impedance  $Z_0$  assumed to be the same for each rib. Each is of length  $l_r$ , thickness  $h_r$ , with material properties  $E_r$  and  $\rho_r$ , and [25]

$$Z_0 = i\rho_r c_r h_r \cot \frac{\omega l_r}{2c_r} \quad (13)$$

where  $c_r = (E_r/\rho_r)^{1/2}$ . Taking the  $k_y$  transform of (12) yields

$$\hat{V}(k_y) = -\hat{Y}(k_y) \left( 4\pi p_0 \delta(k_y - k_n) + q(k_y) \right) \quad (14)$$

where  $\hat{Y}$  is the compliance of the plate and fluid in parallel,

$$\hat{Y}(k_y) = \left( \hat{Z}_p(k_y) + \hat{Z}_f(k_y) \right)^{-1}, \quad (15)$$

with plate impedance according to Kirchhoff theory (or by Eq. (B1) using Mindlin plate theory)

$$\hat{Z}_p(k_y) = \frac{Dk_y^4 - \rho_s h \omega^2}{-i\omega}, \quad (16)$$

and

$$q(k_y) = Z_0 \int_{-\infty}^{\infty} v(y) e^{-i k_y y} \sum_{m=-\infty}^{\infty} \delta(y - y_m) dy. \quad (17)$$

The Poisson Summation identity [21, 26]

$$\sum_{m=-\infty}^{\infty} \delta(y - y_m) = \frac{1}{d} \sum_{m=-\infty}^{\infty} e^{-i 2\pi m \frac{y}{d}} \quad (18)$$

allows us to express Eq. (17) as

$$q(k_y) = \frac{Z_0}{d} \sum_{m=-\infty}^{\infty} \hat{V}(k_y + 2\pi \frac{m}{d}). \quad (19)$$

Noting that  $q(k_y)$  is periodic with period  $2\pi/d$  gives, using Eq. (14),

$$q(k_y) = -4\pi p_0 \hat{Y}(k_n) \hat{Z}(k_0) \sum_{m=-\infty}^{\infty} \delta(k_y - k_m) \quad (20)$$

where

$$\hat{Z}(k_0) = \left( \frac{d}{Z_0} + \sum_{m=-\infty}^{\infty} \hat{Y}(k_m) \right)^{-1}. \quad (21)$$

Equations (10), (14) and (20) yield

$$\begin{aligned} p_s(x, y) &= 2p_0 \hat{Y}(k_n) \left\{ -\hat{Z}_f(k_n) e^{i((k_x)_n x + k_n y)} \right. \\ &\quad \left. + \hat{Z}(k_0) \sum_{m=-\infty}^{\infty} \hat{Z}_f(k_m) \hat{Y}(k_m) e^{i((k_x)_m x + k_m y)} \right\}. \end{aligned} \quad (22)$$

Note that the dispersion relation for symmetric structure-borne waves [10] is  $1/\hat{Z}(k_0) = 0$ .

The total field (8) can now be written, using (22), as

$$p(x, y) = p_0 e^{i(-(k_x)_n x + k_n y)} + p_0 R_p(k_n) e^{i((k_x)_n x + k_n y)} + p_c(x, y) \quad (23)$$

where  $R_p$  is the reflection coefficient for the plate with no constraints,

$$R_p(k_n) = \frac{\hat{Z}_p(k_n) - \hat{Z}_f(k_n)}{\hat{Z}_p(k_n) + \hat{Z}_f(k_n)} \quad (24)$$

and  $p_c$  is caused by the ribs,

$$p_c(x, y) = p_0 \hat{Z}(k_0) \hat{Y}(k_n) \times \sum_{m=-\infty}^{\infty} (1 - R_p(k_m)) e^{i((k_x)_m x + k_m y)}. \quad (25)$$

In summary, referring to Eq. (7), the scattering matrix for symmetric incidence has elements

$$R_{mn}^{(s)} = R_p(k_m) \delta_{mn} + (1 - R_p(k_m)) \hat{Z}(k_0) \hat{Y}(k_n). \quad (26)$$

Acoustical reciprocity [27] is ensured by the symmetry relation  $R_{mn}^{(s)} \hat{Z}_f(k_n) = R_{nm}^{(s)} \hat{Z}_f(k_m)$ .

### B. Symmetric scalar problem: Propagating plane wave incidence

In the special case that the incidence is a plane wave ( $n = 0$ ) then the reflected pressure can be split into two parts: a reflected plane wave and a remainder comprising all modes  $m \neq 0$ . The latter are all evanescent if the frequency is low enough. Specifically,

$$p(x, y) = p_0 e^{i k(-x \cos \theta_0 + y \sin \theta_0)} + p_0 R_{00}^{(s)} e^{i k(x \cos \theta_0 + y \sin \theta_0)} + p_{\text{ev}}^{(s)}(x, y) \quad (27)$$

where the reflection coefficient  $R_{00}^{(s)}$  follows from (26) as

$$R_{00}^{(s)} = \frac{\hat{Z}_{p0}(k_0) - \hat{Z}_f(k_0)}{\hat{Z}_{p0}(k_0) + \hat{Z}_f(k_0)} \quad (28)$$

with modified plate impedance (see (16))

$$\hat{Z}_{p0}(k_0) = \hat{Z}_p(k_0) + \left( \hat{Z}^{-1}(k_0) - \hat{Y}(k_0) \right)^{-1}, \quad (29)$$

and evanescent field

$$p_{\text{ev}}^{(s)}(x, y) = p_0 \hat{Z}(k_0) \hat{Y}(k_0) \times \sum_{m \neq 0} (1 - R_p(k_m)) e^{i((k_x)_m x + k_m y)}. \quad (30)$$

If the frequency is low enough that all of the  $(k_x)_m$  are imaginary except for  $m = 0$  ( $k < \frac{2\pi}{d}(1 + \sin |\theta_0|)^{-1}$ )

then  $p_{\text{ev}}(x, y)$  is evanescent in the  $x$ -direction. The only acoustic energy that radiates to infinity comes from the plane wave. Total energy is conserved if  $|R_{00}| = 1$ , which is the case only if  $\text{Re } Z_0 = 0$ . In the limit of closely spaced ribs ( $d \rightarrow 0$ ) to leading order the sum in (29) is ignorable,  $\hat{Z}_{p0} \approx \hat{Z}_p(k_0) + Z_0/d$ , and (28) agrees with [6, Eq. (32)].

### C. Antisymmetric problem

The total acoustic pressure is assumed to be

$$p(x, y) = -\text{sgn}(x) p_0 \left[ e^{-i((k_x)_n |x| + k_n y)} + \sum_{m=-\infty}^{\infty} R_{mn}^{(a)} e^{i((k_x)_m |x| + k_m y)} \right]. \quad (31)$$

#### 1. An approximate mass dominated solution

The flex-layer moves in the  $x$ -direction as one with velocity  $v_x(0, y) = (i\omega\rho)^{-1} p_{,x}(0, y)$ . The force-acceleration relation can be approximated as

$$-i\omega m_t v_x(0, y) \approx p(-0, y) - p(+0, y), \quad (32)$$

where the total mass density  $m_t$  incorporates the plate and rib masses in a cell-averaged sense,  $m_t = 2\rho_s h + \rho_r h_r l_r / d$  and  $\rho_r$ ,  $h_r$  and  $l_r$  are density, thickness and length of the connecting ribs. The antisymmetric scattering matrix is therefore diagonal with elements

$$R_{mn}^{(a)} \approx \frac{\hat{Z}_{\text{mass}} - \hat{Z}_f(k_m)}{\hat{Z}_{\text{mass}} + \hat{Z}_f(k_m)} \delta_{mn} \quad (33)$$

with mass-like impedance  $\hat{Z}_{\text{mass}} = -\frac{i}{2}\omega m_t$ .

#### 2. Exact solution

As in the symmetric problem we only consider  $x > 0$ , and express the total acoustic pressure in the form (see (8))

$$p(x, y) = -p_0 e^{i(-(k_x)_n x + k_n y)} - p_0 e^{i((k_x)_n x + k_n y)} + p_s(x, y) \quad (34)$$

with additional scattered pressure (10). The plate displacement satisfies (see (12))

$$Dw''''(y) - \rho_s h \omega^2 w(y) = 2p_0 e^{i k_n y} - p_s(0, y) - Z_{0\text{mass}} v(y) \sum_{m=-\infty}^{\infty} \delta(y - y_m). \quad (35)$$

where  $Z_{0\text{mass}}$  is the rib mass impedance

$$Z_{0\text{mass}} = -i \rho_r c_r h_r \tan \frac{\omega l_r}{2c_r}. \quad (36)$$

The solution follows in the same way as for the symmetric problem. Based on eqs. (12), (26) and (31) we find that the exact antisymmetric scattering matrix has elements

$$R_{mn}^{(a)} = R_p(k_m) \delta_{mn} + (1 - R_p(k_m)) \hat{Z}_{\text{mass}}(k_0) \hat{Y}(k_n) \quad (37)$$

where, see (21),

$$\hat{Z}_{\text{mass}}(k_0) = \left( \frac{d}{Z_{0\text{mass}}} + \sum_{m=-\infty}^{\infty} \hat{Y}(k_m) \right)^{-1}. \quad (38)$$

It may be shown that (37) reduces to the mass dominated approximation (33) as  $\omega \rightarrow 0$ . Also, the dispersion relation for anti-symmetric structure-borne waves is  $1/\hat{Z}_{\text{mass}}(k_0) = 0$ .

#### D. Scattering of an incident wave from a flex-layer

A wave is incident from  $x < 0$  only, with total acoustic pressure

$$p(x, y) = p_0 \times \begin{cases} [e^{i((k_x)_n x + k_n y)} \\ + \sum_{m=-\infty}^{\infty} R_{mn} e^{i(-(k_x)_m x + k_m y)}], & x < 0, \\ \sum_{m=-\infty}^{\infty} T_{mn} e^{i((k_x)_m x + k_m y)}, & x > 0. \end{cases} \quad (39)$$

Combining the two separate solutions in Eq. (7) and (31) the reflection and transmission matrices follow as

$$R_{mn} = \frac{1}{2} (R_{mn}^{(s)} + R_{mn}^{(a)}). \quad T_{mn} = \frac{1}{2} (R_{mn}^{(s)} - R_{mn}^{(a)}). \quad (40)$$

Hence,

$$R_{mn} = \frac{1}{2} (\hat{Z}(k_0) + \hat{Z}_{\text{mass}}(k_0)) (1 - R_p(k_m)) \hat{Y}(k_n) + R_p(k_m) \delta_{mn}, \quad (41)$$

$$T_{mn} = \frac{1}{2} (\hat{Z}(k_0) - \hat{Z}_{\text{mass}}(k_0)) (1 - R_p(k_m)) \hat{Y}(k_n).$$

The above general solution is valid for propagating and evanescent incident waves. In the special case of a single propagating incident plane wave at low frequency, we have

$$p(x, y) = \begin{cases} p_0 e^{i k(x \cos \theta_0 + y \sin \theta_0)} \\ + R_{00} p_0 e^{i k(-x \cos \theta_0 + y \sin \theta_0)} + p_{\text{ev}}(x, y), & x < 0, \\ T_{00} p_0 e^{i k(x \cos \theta_0 + y \sin \theta_0)} + p_{\text{ev}}(x, y), & x > 0 \end{cases} \quad (42)$$

where

$$p_{\text{ev}}(x, y) = p_0 \sum_{m \neq 0} e^{i k_m y} \times \begin{cases} R_{mn} e^{-i(k_x)_m x}, & x < 0, \\ T_{mn} e^{i(k_x)_m x}, & x > 0. \end{cases} \quad (43)$$

Energy conservation requires that  $|R_{00}|^2 + |T_{00}|^2 = 1$ .

#### IV. VERIFICATION AND ANALYSIS OF THE FLEX-LAYER MODEL

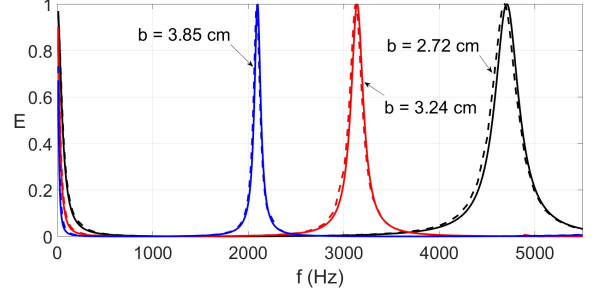


FIG. 6. The transmitted acoustic energy  $E$  vs frequency for three different flex-layers each with 1 mm Aluminum plates. Solid lines and dashed lines are obtained using Eq. (40) and COMSOL, respectively.

The transmitted acoustic energy  $E = |T_{00}|^2$  plotted in Fig. 6 shows that the theoretical result agrees with full FEM simulation. Three different flex-layers are considered with rib spacing parameter  $b$  corresponding to air gaps of width  $d_a = 0.5, 1,$  and  $2$  mm, see Fig. 3. The plots in Fig. 6 again verify the equivalence of the flex-layer to the air gaps in the low frequency range.

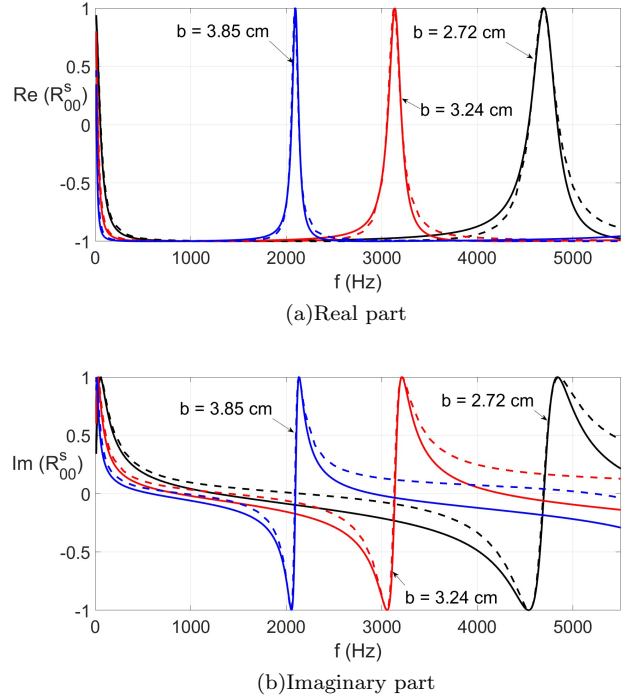


FIG. 7. Comparison of the symmetric reflection coefficient  $R_{00}^{(s)}$  vs frequency for the flex-layer with 1 mm plates. Solid lines and dashed lines are obtained using Eq. (26) and COMSOL, respectively.

The equivalence is true up to at least 1 kHz. However,

Fig. 6 illustrates a new phenomenon of total transmission at frequencies in the range 2 to 5 kHz. These values are much less than the lowest frequencies expected for total transmission through the air-gaps, i.e. at  $f = \frac{c_a}{2d_a}$  which are approximately twenty times as large as those of Fig. 6.

The transmission frequencies of Fig. 6 can be understood by noting that the antisymmetric reflection coefficient  $R_{00}^{(a)}$  of Eq. (33) is approximately  $-1$ , indicating that  $E$  of Eq. (40) equals 1 when  $R_{00}^{(s)} = 1$ , or equivalently  $R_{00} = 0$ . This is borne out by comparing the results of Fig. 7 with those of Fig. 6.

Referring to Eq. (28), the coefficient  $R_{00}^{(s)} = 1$  when  $\hat{Z}_{p0} \rightarrow \infty$ . Equation (29) implies this occurs when  $\sum_{m \neq 0} \hat{Y}(k_m) = 0$ . Assuming normal incidence ( $\theta_0 = 0$ ) this can be expressed as

$$\sum_{m=1}^{\infty} \left( m^4 \xi^4 - \Omega^2 - \frac{\epsilon \Omega^2}{\sqrt{m^2 \xi^2 - \Omega^2}} \right)^{-1} = 0 \quad (44)$$

with non-dimensional frequency  $\Omega = \omega/\omega_c$  and

$$\omega_c = c^2 \sqrt{\frac{\rho_s h}{D}}, \quad \epsilon = \frac{\rho c}{\rho_s h \omega_c}, \quad \xi = \frac{2\pi c}{d \omega_c}. \quad (45)$$

Here  $\omega_c$  is the coincidence frequency at which the phase velocity of the bare plate flexural wave coincides with  $c$ , and  $\epsilon$  is a common non-dimensional measure of fluid loading [28]. Note that the related sum  $\sum_{m=-\infty}^{\infty} \hat{Y}(k_m)$  can be asymptotically approximated under the heavy fluid loading limit [10] for which  $(\rho \omega^2/D)^{\frac{1}{5}} \gg k_0$  and  $(\rho \omega^2/D)^{\frac{1}{5}} \gg (\rho_s h \omega^2/D)^{\frac{1}{4}}$ . This limit is, however, not relevant to the parameters considered here.

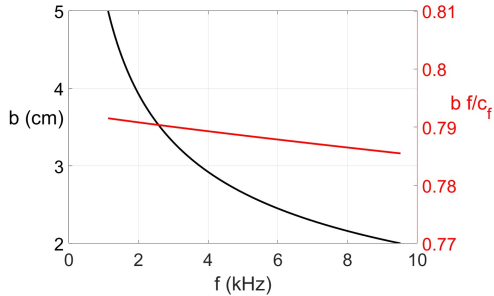


FIG. 8. Two views of the full transmission frequency of the flex-layer, noted in Fig. 6 for three values of the rib separation parameter  $b$ . The black curve (left) shows  $b$  as a function of the full transmission frequency using Eq. (44), i.e.  $\sum_{m \neq 0} \hat{Y}(k_m) = 0$ ; the red curve (right) is the non-dimensional measure  $b f / c_f$  where  $c_f$  is the fluid-loaded plate phase velocity obtained from Eq. (46), i.e.  $1/\hat{Y}(k_y) = 0$ .

The physical origin of the transmission frequencies of Fig. 6 is actually the reverberation of fluid-loaded flexural waves, see Fig. 8. The fluid-loaded flexural wave-number  $k_y$  is the solution of  $\hat{Z}_p(k_y) + \hat{Z}_f(k_y) = 0$ , which can be expressed in terms of the flexural wave phase velocity  $c_f = \omega/k_y$  as  $\tau = \sqrt{c^2/c_f^2 - 1}$ , the positive root of [28, Eq. (8.8)]

$$\tau^5 + 2\tau^3 + (1 - \Omega^{-2})\tau - \epsilon \Omega^{-3} = 0. \quad (46)$$

Figure 8 shows that the non-dimensional rib parameter  $b f / c_f$  is approximately constant over a ten-fold range of frequency, indicating that the transmission peak is associated with flexural waves bouncing back and forth between ribs. The small variation of  $b f / c_f$  between 1 and 10 kHz can be attributed to frequency dependent interaction of the plate wave with the ribs. Numerical solution of  $c_f$  in Eq. (46) versus frequency is shown in Fig. (9) along with an explicit approximate solution “ $\gamma = k_f$ ” [28, Eq. (8.10)].

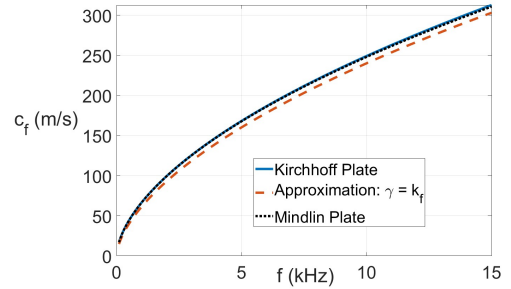


FIG. 9. Flexural wave phase velocity  $c_f$  vs frequency

Finally, the scattered velocity in the vicinity of the flex-layer is shown in Fig. 10 where

$$V_x^{sc}(x, y) = \frac{1}{i \omega \rho} \frac{\partial p_s}{\partial x}(x, y), \quad V_y^{sc}(x, y) = \frac{1}{i \omega \rho} \frac{\partial p_s}{\partial y}(x, y). \quad (47)$$

Note the similarity of the velocity profiles even as the rib spacing  $b$  and frequency  $f$  change.



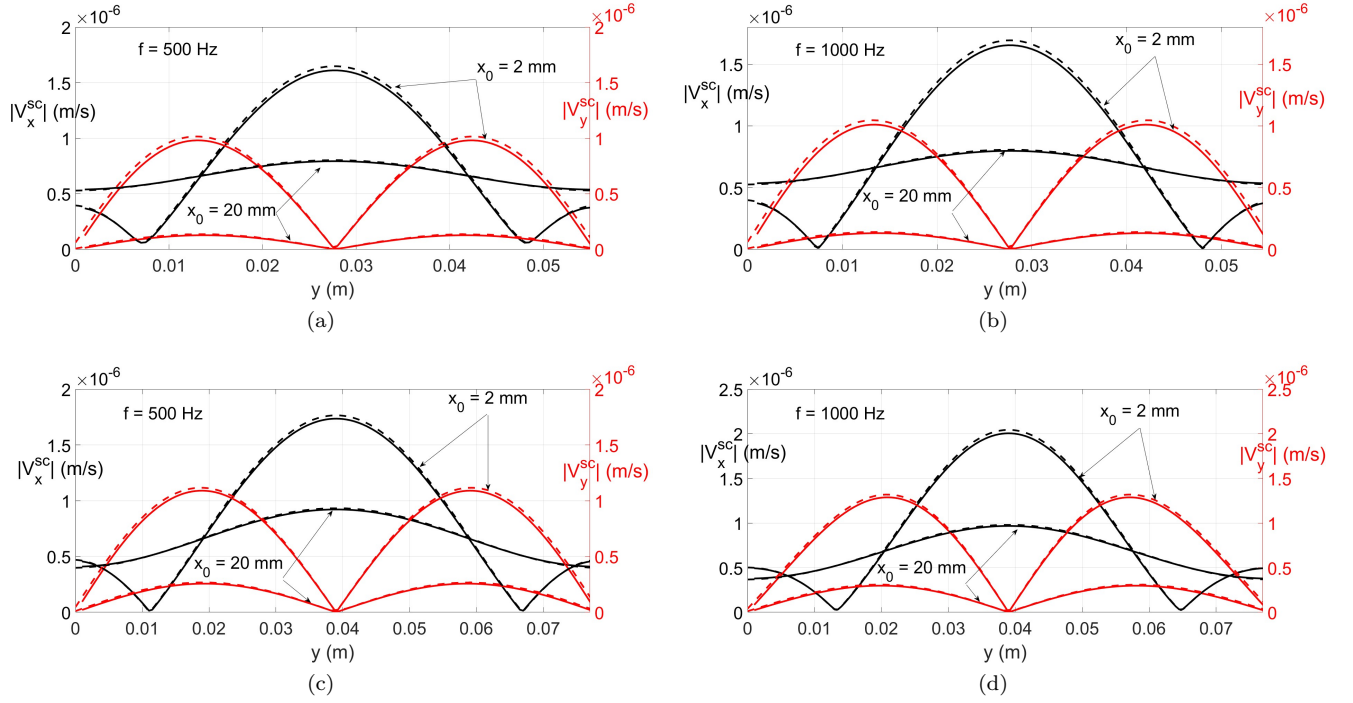


FIG. 10. Magnitude of scattered velocities in  $x$  and  $y$  directions measured at a plane a distance of  $x_0$  from the flex-layer. Solid lines and dashed lines are obtained using Eq. (47) and COMSOL, respectively.  $p_0 = 1$  Pa, (a,b)  $b = 2.72$  cm, (c,d)  $b = 3.85$  cm

## V. MULTIPLE FLEX-LAYERS IN SERIES: $n = 2$

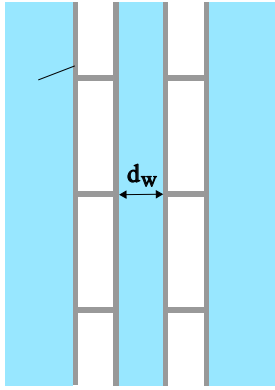


FIG. 11. Two flex-layers in series separated by a water gap of width  $d_w$ .

Consider two flex-layers separated by a gap as shown in Fig. 11. A plane wave incident from the left or the right will generate an infinite set of evanescent waves in the gap, which will in turn reverberate between the flex-layers. However, the full transmission and reflection solution can be found in a semi-analytic form using the fundamental solution for the single flex-layer of Eqs. (39) and (40). The multiple scattering solution can be found

by analogy with the scalar, or single wave, multiple scattering problem.

Since the flex-layer converts a plane wave into the infinite reflected and transmitted constituents we work with infinite vectors  $\mathbf{u}^+$  and  $\mathbf{u}^-$  corresponding to propagation in the positive and negative  $x$ -directions. We consider a propagating plane wave incident from the left,  $\mathbf{u}_0^+$ , where  $\{u_0^+\}_m = \delta_{m0}$ . The wave reflected from a single flex-layer is  $\mathbf{R}\mathbf{u}_0^+$ , and the transmitted wave is  $\mathbf{T}\mathbf{u}_0^+$  where  $\mathbf{R}$  and  $\mathbf{T}$  are the infinite matrices defined by Eqs (40).

The full transmission and reflection from the two flex-layers in series follows from a ray summation approach. The wave transmitted to the right, and the wave reflected to the left are, respectively,

$$\begin{aligned} \mathbf{u}^+ &= \mathbf{T}(\mathbf{1} + \mathbf{A} + \mathbf{A}^2 + \dots)\mathbf{P}\mathbf{T}\mathbf{u}_0^+, \\ \mathbf{u}^- &= \mathbf{R}\mathbf{u}_0^+ + \mathbf{TPR}(\mathbf{1} + \mathbf{A} + \mathbf{A}^2 + \dots)\mathbf{P}\mathbf{T}\mathbf{u}_0^+, \end{aligned} \quad (48)$$

where  $\mathbf{P}$  is the propagator matrix through the water layer of thickness  $d_w$ , with  $\{P\}_{mn} = e^{i d_w (k_x)_m} \delta_{mn}$ , and  $\mathbf{A} = (\mathbf{PR})^2$ . Hence,

$$\begin{aligned} \mathbf{u}^+ &= \mathbf{T}(\mathbf{1} - \mathbf{A})^{-1}\mathbf{P}\mathbf{T}\mathbf{u}_0^+, \\ \mathbf{u}^- &= \mathbf{R}\mathbf{u}_0^+ + \mathbf{TPR}(\mathbf{1} - \mathbf{A})^{-1}\mathbf{P}\mathbf{T}\mathbf{u}_0^+. \end{aligned} \quad (49)$$



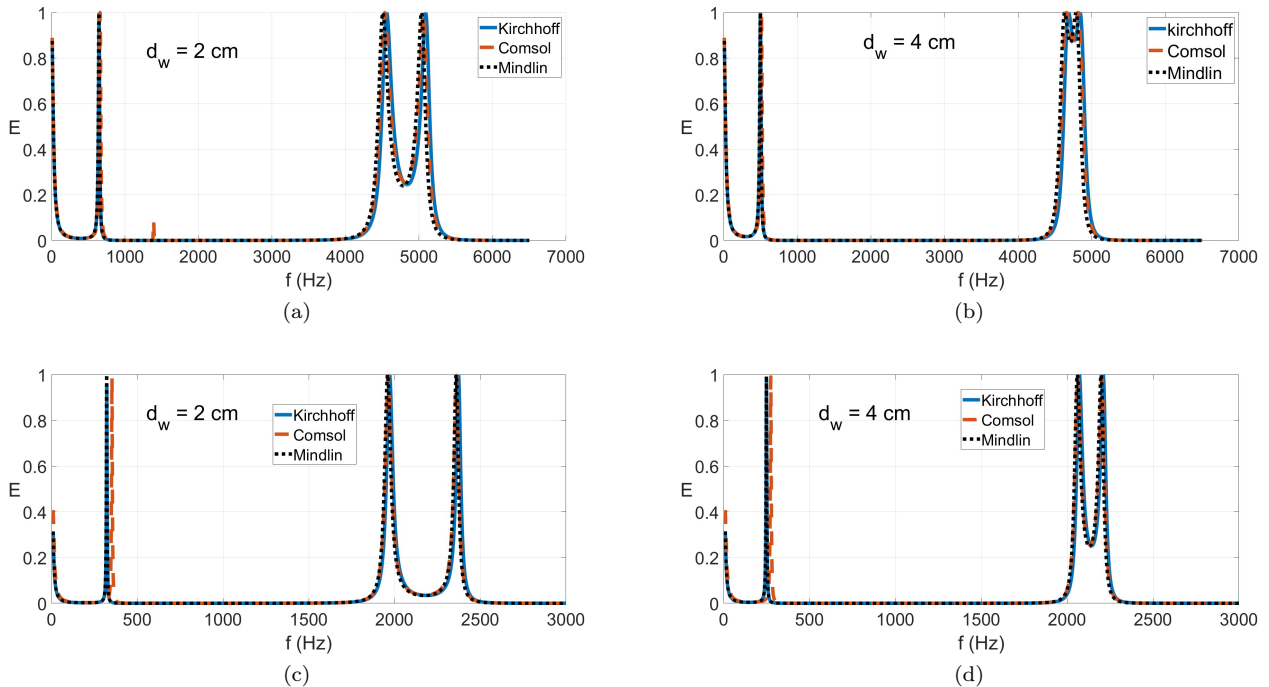


FIG. 12. The transmitted acoustic energy  $E$  vs frequency for the 2-Flex-layer model with a distance of  $d_w$  from each other. The Aluminum plate thickness is considered 1 mm. (a,b)  $b = 2.72$  cm, (c,d)  $b = 3.85$  cm

Figure (12) shows the total transmitted energy (normalized to unity for incident). The theory based on Kirchhoff and Mindlin models are compared with Comsol simulations. The theoretical transmission coefficient  $E$  is the propagating component of  $\mathbf{u}^+$ , that is

$$E = T_{00} = \mathbf{u}_0^+{}^T \mathbf{u}^+. \quad (50)$$

Comparing Figs. (12) and (6) for  $E$  reveals noticeable differences. It is observed that the first mode appears at lower frequencies in Fig. (12). This observation can be explained by considering that the water between two flex structures has an equivalent mass, and the flex structures themselves possess equivalent mass and stiffness. Consequently, the first resonance of the 2-flex-layer model is formulated as  $f_1 \approx \frac{1}{2\pi} \sqrt{\frac{2k_f}{2m_f + M_w}}$ . In addition to the low frequency transmission, Fig. 12 also shows that the transmission modes of the single flex-layer, see Fig. 6, bifurcate into double transmission peaks. The separation of the double peaks depends upon the spacing  $d_w$  between the flex-layers, with larger separation for smaller  $d_w$ . This phenomenon is related to the presence of “evanescent pressure” between the two flexible layers, which creates diffused angles of reflection on each flex-layer. The bifurcation can also be interpreted as a “level splitting” effect due to the extra degree of freedom in the  $n = 2$  system.

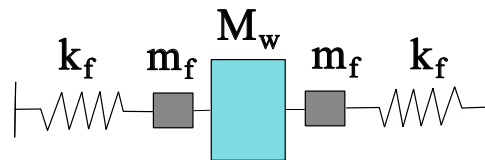


FIG. 13. Simplified 2-flex-layer model for the mode  $m = 1$

## VI. SUMMARY AND CONCLUSIONS

The spatially periodic nature of the flex-layer causes it to generate an infinite set of evanescent waves under plane wave incidence. By solving for generalized Bragg wave incidence we have derived an analytical method to consider scattering from multiple flex-layers in series. Although we have here restricted attention to the  $n = 2$  case it is clear that the method can be developed for an arbitrary number of flex-layers by analogy with the purely one-dimensional case. The solution is based on the explicit infinite-dimensional reflection and transmission matrices of Eq. (40). The scalar elements  $R_{00}$  and  $T_{00}$  provide the amplitudes of the far-field propagating reflected and transmitted waves. The other elements define the evanescent contributions to the acoustic near-field.

We have shown that the low frequency response of the flex-layer in water is analogous to that of a simple spring, which can be interpreted specifically in terms of an equiv-

alent air gap. Conversely, the flex-layer could be used to replace an air gap of given width in the sense of lumped acoustic elements. The flex-layer exhibits total transmission (zero reflection) at finite frequencies defined by relation (44). While this must be solved numerically to find transmission frequencies, we have identified the lowest one as  $f \approx 0.79 c_f/b$  where  $2b$  is the rib spacing and  $c_f$  is the phase speed of the dispersive fluid-loaded flexural wave, see Figs. 8 and 9.

Finally, we have demonstrated the acoustic properties of two flex-layers in series, illustrating new effects not seen in the single flex-layer. The mode splitting exhibited in Fig. 12 can be controlled by the choice of the water separation between the flex-layers, leading to wider total transmission peaks. This suggests that interesting broadband effects can be expected with multiple flex-layers, such as broadband total transmission with the potential for new applications in acoustic metamaterials. Future work will examine multiple flex-layer systems, based upon the reflection and transmission for the single layer introduced in this paper.

#### Appendix A: Quasi-static solution using Timoshenko theory

Instead of the Euler-Bernoulli theory (1) we use the Timoshenko theory

$$D\phi'''(y) = p_0, \quad w'(y) = \phi - \frac{D}{\mu h \kappa} \phi'', \quad (\text{A1})$$

for  $-b \leq y \leq b$  where  $\mu$  is the shear modulus and  $\kappa$  is a shear correction factor. Solving for the rotation  $\phi(y)$  and

plate deflection  $w(y)$  and setting  $w(\pm b) = 0$  and  $\phi(\pm b) = 0$ , gives  $w(y) = w_{\text{EB}}(y) + p_0 (b^2 - y^2)/(2\mu h \kappa)$  where  $w_{\text{EB}}$  is the deflection found in Section II using Euler-Bernoulli beam theory. The magnitude of the deflection is therefore larger than that of the Euler-Bernoulli solution and yields

$$\Delta L = \frac{2}{45} \frac{b^4}{D} p_0 \left( 1 + \frac{5h^2}{2b^2 \kappa (1 - \nu)} \right) \quad (\text{A2})$$

where we have used  $E_p = 2\mu(1 + \nu)$ . This  $\Delta L$  is slightly greater as compared to that of Eq. (2), although the relative correction is on the order of  $10^{-3}$  for the values considered here. In conclusion, Timoshenko theory gives very little difference for the frequencies considered.

#### Appendix B: Mindlin plate model

Using the Mindlin plate theory [6] changes  $\hat{Z}_p$  from (16) to

$$\hat{Z}_p(k_y) = \frac{(Dk_y^2 - \lambda \rho_s I \omega^2)(k_y^2 - \frac{\rho_s \omega^2}{\kappa \mu}) - \rho_s h \omega^2}{-i \omega \left( 1 + \frac{Dk_y^2 - \lambda \rho_s I \omega^2}{\kappa \mu h} \right)} \quad (\text{B1})$$

where  $\mu (= \frac{E_p}{2(1+\nu)})$  is the shear modulus,  $\kappa$  is a shear correction factor and  $\lambda$  is rotary inertia correction factor. Following [29] we take  $\lambda = \kappa/\kappa_0$  and  $\kappa = \frac{20}{17-7\nu} / \left( 1 + \sqrt{1 - \frac{200(1-\nu)}{\kappa_0(17-7\nu)^2}} \right)$  where  $\kappa_0 = \pi^2/12$ .

- 
- [1] G. F. Lin, S. I. Hayek, Acoustic radiation from point excited rib-reinforced plate, *Journal of the Acoustical Society of America* 62 (1) (1977) 72–83. doi:10.1121/1.381506.
  - [2] B. L. Woolley, Acoustic scattering from a submerged plate. I. One reinforcing rib, *Journal of the Acoustical Society of America* 67 (5) (1980) 1642–1653. doi:10.1121/1.384287.
  - [3] E. A. Skelton, Acoustic scattering by parallel plates with a single connector, *Proceedings of the Royal Society of London. A. Mathematical and Physical Sciences* 427 (1873) (1990) 401–418. doi:10.1098/rspa.1990.0020.
  - [4] I. V. Andronov, B. P. Belinskiy, Acoustic scattering from an elastic plate supported by a rigid narrow rib, *Wave Motion* 35 (4) (2002) 277–287. doi:10.1016/s0165-2125(01)00105-6.
  - [5] B. L. Woolley, Acoustic scattering from a submerged plate. II. Finite number of reinforcing ribs, *Journal of the Acoustical Society of America* 67 (5) (1980) 1654–1658. doi:10.1121/1.384288. URL <http://dx.doi.org/10.1121/1.384288>
  - [6] P. Stepanishen, The acoustic transmission and scattering characteristics of a plate with line impedance discontinuities, *Journal of Sound and Vibration* 58 (2) (1978) 257–272. doi:10.1016/s0022-460x(78)80080-7.
  - [7] A. K. Karali, Acoustic scattering from infinite elastic plates with periodic reinforcements, Ph.D. thesis, The Pennsylvania State University (1994).
  - [8] B. A. Cray, Acoustic radiation from periodic and sectionally aperiodic rib-stiffened plates, *Journal of the Acoustical Society of America* 95 (1) (1994) 256–264. doi:10.1121/1.408358. URL <http://dx.doi.org/10.1121/1.408358>
  - [9] F. Xin, T. Lu, Transmission loss of orthogonally rib-stiffened double-panel structures with cavity absorption, *The Journal of the Acoustical Society of America* 129 (4) (2011) 1919–1934.
  - [10] E. A. Skelton, R. V. Craster, A. Colombi, D. J. Colquitt, The multi-physics metawedge: graded arrays on fluid-loaded elastic plates and the mechanical analogues of rainbow trapping and mode conversion, *New Journal of Physics* 20 (5) (2018) 053017. doi:10.1088/1367-2630/aabecf.

- [11] R. F. Keltie, Structural acoustic response of finite rib-reinforced plates, *Journal of the Acoustical Society of America* 94 (2) (1993) 880–887. doi:10.1121/1.408188.
- [12] M. Tran-Van-Nhieu, G. Maze, D. Décultot, Approximate solutions to acoustic scattering from a ribbed finite plate, *Journal of the Acoustical Society of America* 141 (5) (2017) 3091–3100. doi:10.1121/1.4982039.
- [13] S. Wrona, M. Pawelczyk, X. Qiu, Shaping the acoustic radiation of a vibrating plate, *Journal of Sound and Vibration* 476 (2020) 115285. doi:10.1016/j.jsv.2020.115285.
- [14] J. Ye, Y. Sun, Analysis of the vibro-acoustic behaviours of underwater reinforced rectangular plates, *Journal of Physics: Conference Series* 2285 (1) (2022) 012027. doi:10.1088/1742-6596/2285/1/012027.
- [15] A. J. Hull, J. R. Welch, Elastic response of an acoustic coating on a rib-stiffened plate, *Journal of Sound and Vibration* 329 (20) (2010) 4192–4211. doi:10.1016/j.jsv.2010.04.012.
- [16] M. C. Remillieux, R. A. Burdisso, Vibro-acoustic response of an infinite, rib-stiffened, thick-plate assembly using finite-element analysis, *Journal of the Acoustical Society of America* 132 (1) (2012) EL36–EL42. doi:10.1121/1.4730029.
- [17] F. Xin, An exact elasticity model for rib-stiffened plates covered by decoupling acoustic coating layers, *Composite Structures* 119 (2015) 559–567. doi:10.1016/j.compstruct.2014.09.024.
- [18] G.-F. Lin, J. M. Garrelick, Sound transmission through periodically framed parallel plates, *The Journal of the Acoustical Society of America* 61 (4) (1977) 1014–1018.
- [19] J. Wang, T. Lu, J. Woodhouse, R. Langley, J. Evans, Sound transmission through lightweight double-leaf partitions: theoretical modelling, *Journal of Sound and Vibration* 286 (4-5) (2005) 817–847.
- [20] M. L. Rumerman, Vibration and wave propagation in ribbed plates, *The Journal of the Acoustical Society of America* 57 (2) (1975) 370–373. doi:10.1121/1.380450.
- [21] V. N. Evseev, Sound radiation from an infinite plate with periodic inhomogeneities, *Sov. Phys. Acoust.* 19 (1973) 226–229.
- [22] B. Mace, Sound radiation from a plate reinforced by two sets of parallel stiffeners, *Journal of Sound and Vibration* 71 (3) (1980) 435–441.
- [23] D. Takahashi, Sound radiation from periodically connected double-plate structures, *Journal of Sound and Vibration* 90 (4) (1983) 541–557. doi:10.1016/0022-460x(83)90810-6.
- [24] E. A. Skelton, Acoustic scattering by parallel plates with periodic connectors, *Proceedings of the Royal Society of London. A. Mathematical and Physical Sciences* 427 (1873) (1990) 419–444. doi:10.1098/rspa.1990.0021.
- [25] S. S. Rao, *Vibration of Continuous Systems*, John Wiley & Sons, 2019.
- [26] A. Zygmund, *Trigonometric Series*, 3rd Edition, Cambridge Mathematical Library, Cambridge University Press, 2003.
- [27] H. Nassar, B. Yousefzadeh, R. Fleury, M. Ruzzene, A. Alù, C. Daraio, A. N. Norris, G. Huang, M. R. Haberman, Nonreciprocity in acoustic and elastic materials, *Nature Reviews Materials* 5 (9) (2020) 667–685. doi:10.1038/s41578-020-0206-0.
- [28] M. C. Junger, D. Feit, *Sound, Structures, and Their Interaction*, MIT Press, Cambridge, MA, 1986.
- [29] A. N. Norris, A refinement of Mindlin plate theory using simultaneous rotary inertia and shear correction factors, *Journal of Vibration and Acoustics* 140 (3) (2018) 034503. doi:10.1115/1.4038956.